Modeling and Design of a Pigeon-Inspired Robot With Passively Bending Wings

Shi Zhang, Yishi Shen, Weimin Huang, Chengrui Shang, Wenjie Chen, and Qing Shi, *Senior Member, IEEE*

***Abstract*—Most traditional ornithopters are equipped with active deformation wings for flight control. However, this inevitably results in redundant actuators and a complex mechanical structure, that reduce flight efficiency. According to the flight data of pigeons (*Columba livia*), we propose a simple but subtly designed robot that has a passively bending leading-edge spar of the wing and no need for redundant actuators. Accordingly, a double pendulum with a spring system was used to mimic the passive bending of the pigeon's forearm muscles during the upstroke and downstroke. Furthermore, by analyzing the longitudinal flight dynamics, we found that the passive bending of wings increases lift, which relates to flight maneuverability, by changing the effective wing area. Finally, we conducted experiments on wing kinematics, lift/thrust generation, power consumption, and properties of the compliant revolute joint for three springs with different stiffness. The experimental results show that the optimal design of our robot generates a lift of 1.8 times the take-off weight, which is superior to the performance of existing state-of-the-art pigeon-scale ornithopters (wingspan: approx. 600 mm). In addition, its energy consumption is 38.2% lower than that of existing pigeon-scale ornithopters. Moreover, free-flight tests show that the asymmetry bending angle due to the compliant revolute joint effectively improves flight maneuverability.**

***Index Terms*—Biologically inspired robot, biomimetics, mechanism design.**

Manuscript received 1 March 2023; accepted 15 June 2023. Date of publication 5 July 2023; date of current version 17 July 2023. This letter was recommended for publication by Associate Editor J. Liu and Editor X. Liu upon evaluation of the reviewers' comments. This work was supported in part by the National Natural Science Foundation of China under Grant 61933001 and in part by the National Natural Science Foundation of China under Grant U2013208. *(Corresponding author: Wenjie Chen.)*

This work involved human subjects or animals in its research. Approval of all ethical and experimental procedures and protocols was granted by Experimental Animal Welfare Ethics Review Committee, Institute of Zoology, Chinese Academy of Sciences under Application No. IOZ-IACUC-2023-081, and performed in line with the Measurement of body posture adjustment in birds during locomotion.

Shi Zhang, Yishi Shen, Weimin Huang, and Qing Shi are with the Key Laboratory of Biomimetic Robots and Systems, Beijing Institute of Technology, Ministry of Education, Beijing 100081, China, and also with the Intelligent Robotics Institute, School of Mechatronical Engineering, Beijing Institute of Technology, Beijing 100081, China (e-mail: 3220215041@bit.edu.cn; 3120225086@bit.edu.cn; 3220220174@bit.edu.cn; shiqing@bit.edu.cn).

Chengrui Shang is with the Institute of Zoology, Chinese Academy of Sciences, Beijing 10081, China (e-mail: shangchengrui21@ioz.ac.cn).

Wenjie Chen is with the State Key Lab of Intelligent Control and Decision of Complex Systems, Beijing Institute of Technology, Beijing 10081, China, and also with the School of Automation, Beijing Institute of Technology, Beijing 100081, China (e-mail: chen.wenjie@163.com).

Digital Object Identifier 10.1109/LRA.2023.3292578

I. Introduction

BIRDS morph their wings during flight to adapt to different environments [1], [2]. The anatomy of bird joints allows for different degrees of freedom; e.g., birds can perform flapping, twisting, sweeping, bending and other flexible movements using their muscles and changing the angles of the skeletal joints [3], [4].

In gliding at high speed, birds tend to contract their wrists and sweep their wings backward to dramatically reduce the wing area, ultimately increasing vertical stability and conserving energy [5], [6], [7]. In contrast, during flapping, the elbow folds back and the wrist flexes to improve flight maneuverability, especially in high-frequency flapping [4], [8], [9]. Studies have shown that birds alter forces and moments by bending the wing to reduce the vertical area, thereby creating asymmetries in the downstroke and upstroke [10]. These asymmetries affect the stability of a bird's body, which affects the flight performance [11]. Studying the wing morphing of birds in flight thus provides insights for the wing design of unmanned aerial vehicles, especially flapping-wing robots.

Observations of the flapping of birds have shown that passive morphing is a more important deformation mode than active morphing [12]. Passive morphing is considered to be the most energy-efficient way to morph wings in improving flight performance. The design of flapping-wing robots built to mimic the structure and function of bird wings is thus becoming a research hotspot. David et al. used coiled springs as connecting joints in designing a morphing wing. They conducted a static test to confirm the generation of greater lift by the passive morphing of wings [13]. The Festo Smart-Bird, designed with passive torsion joints, has demonstrated the feasibility of passive joint design in ornithopters. In addition, measurements have been made using a carousel-type device to verify energy savings [14]. Yashwanth et al. verified the effect of asymmetric flapping on the flight performance of an ornithopter that achieved passive deformation during the upstroke and downstroke through unique joints applied to the leading edge of the wing [15]. Cristina et al. designed a biased torsional spring with a rigid joint for bending, providing a functional enhancement of the ornithopter's payload capacity. The proposed optimization model was verified by confirming an increase in lift and a decrease in power consumption [16]. The improved flight performance of the passive bending ornithopter has been proposed. However, owing to a lack of understanding of the lift mechanisms resulting from the unsteady aerodynamics

TABLE I
PERFORMANCE OF PASSIVE MORPHING ORNITHOPTERS

Refs.	Force	Energy consumption	Verification
[13]	Lift improved 10times, Lift/take-off-weight=0.1	-	Bench
[15], [18]	Horizontal thrust coefficient increase 300%	No additional power expenditure	Bench and Flight in Fixed Tail
[16]	Lift increase 16%, Lift/take-off-weight=1.1	Decreases 10%	Free Flight
This work	Lift increase 22.3%, Lift/take-off-weight=1.8	Decreases 38.2%	Bench and Free Flight

of the flapping-wing motion, the above-mentioned method of optimizing the wing design faces the problems of insufficient lift and poor maneuverability.

Meanwhile, we were inspired by research on the remarkable flight capabilities of pigeons [17], such as flexible predator avoidance and long-distance flight. We thus collected data on joints for the flapping of pigeons(*Columba livia*)through motion capture and designed a flapping-wing robot having the same size as the pigeon, focusing on the flapping angle and bending position. We also analyzed the principles of skeletal and muscle movement, and inserted a compliant revolute joint (CRJ) with three springs of different stiffness into the leading-edge spar of the wing to investigate the mechanism by which the passive bending of a wing affects lift from a bionic perspective.

The novelty of the proposed ornithopter is that 1) the mechanical design is inspired by pigeon flight data and 2) muscle is simulated using three springs with different stiffness. Longitudinal flight dynamics combined with wing kinematics metrics show that, unlike other wing deformations (such as twisting), the dominant factor for greater lift in the passive bending of the wing is the reduction of the effective wing area during the upstroke. A lift generation experiment and an energy consumption experiment show that the best solution (labelled $k2$) of the proposed ornithopter requires 1.52 W of electrical power to generate 271.77 g of lift. Compared with the case for rigid wings, the lift is increased by 22.3% and the energy consumption is reduced by 38.2%. Furthermore, adopting a system of a double pendulum with a spring, we obtain the optimal lift by calculating the passive bending angle according to the spring stiffness. Our design method can easily be extended to the design of other pigeon-inspired ornithopters. The above performance is mainly the result of the use of pigeon flight data as prior knowledge; e.g., the flapping amplitude and bending position are derived from pigeons (*Columba livia*). In addition, the pigeon forelimb muscle model is used to derive a double pendulum with a spring system, which can be used to calculate the optimal spring stiffness.

Several state-of-the-art ornithopters are compared with our best design (labelled $k2$) in Table I. In summary, a search of the literature on ornithopters capable of passive deformation shows that few systems have been demonstrated in free flight owing to insufficient lift, which is an important indicator of flight capability. In particular, compared with E-Flap, the most advanced passive-bending-wing ornithopter capable of free flight, the proposed robot has better performance in terms of the lift-to-take-off-weight ratio (1.8 vs. 1.1). The proposed ornithopter thus generates more lift per unit mass than existing passive morphing ornithopters.

The remainder of the article is organized as follows. Section II presents the design process of the ornithopter. In Section III, a flight dynamic model with a forearm double pendulum with a spring model is described. In Section IV, we conduct a wing kinematics experiment, lift/thrust generation experiment, energy consumption experiment, and free-flight experiment to evaluate the performance of the prototype. Section V provides concluding remarks.

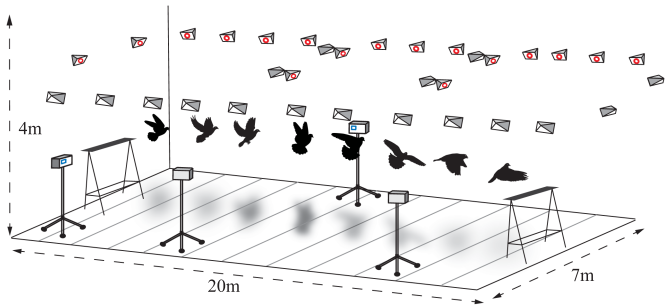

Fig. 1. Experimental setup of the flight laboratory.

TABLE II
GEOMETRY DATA OF THE PIGEON-INSPIRED ROBOT

Parameters	Value
Inner Wingsemi-span	0.207 m
Outer Wingsemi-span	0.103 m
Aspect ratio	1.95
Flapping Amplitude	96°

II. SYSTEM DESIGN

A. Collection of Pigeon Flight Data

The skeleton of the pigeon's wing is similar to that of the human upper limb, comprising humerus, ulna, radius, and carpal bones. The wrist joint and triangular area of the feather membrane between the wrist and shoulder joints form the leading edge of the wing. Three pigeons (*Columba livia*) with a wingspan of approximately 600 mm and an average weight of 360 g were selected as subjects. As shown in Fig. 1, the flight laboratory was 20 m long, 7 m wide, and 4 m high and was equipped with 30 Opti-track infrared cameras, while four action cameras were used to record the flight. The pigeon took off and landed between two perches. Eight marker points were attached to the pigeon for motion analysis; i.e., two shoulder markers, two elbow markers, two wrist markers, and two metacarpal markers. We only considered the markers on the shoulders and wrists in this study. The trajectories of the four considered markers during a wingbeat are shown in Fig. 2.

This trajectory shows an asymmetric deformation of the wrist joint during the upstroke and downstroke in flapping flight, eventually leading to the bending of the leading edge of the wing. As given in Table II, the wingspan of the wrist-inspired

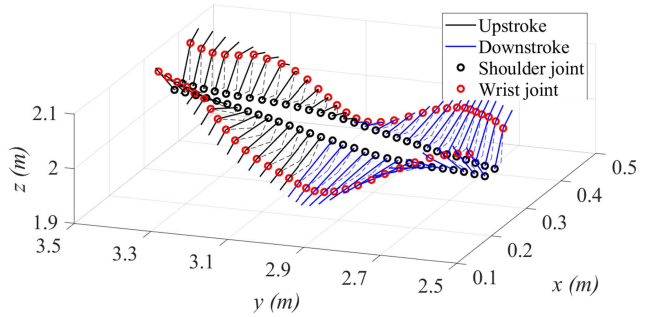

Fig. 2. Trajectory of pigeon joint motion.

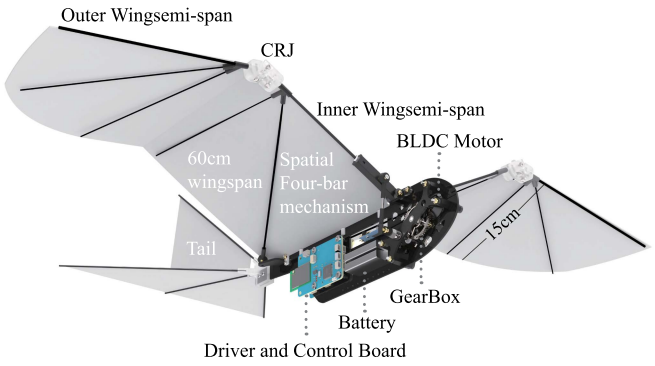

Fig. 3. Ornithopter design and subsystem configuration.

wing was set at 0.6 m, the area of the wing surface was set at 0.41 m^2, the wrist joint was located at 67% of the wing half span, and the flapping amplitude was set 96°, which are values similar to the biological counterparts.

B. Prototype Fabrication

As shown in Fig. 3, our ornithopter is equipped with a brushless DC (BLDC) motor that drives the flapping and a conventional T-tail. The body frame of the ornithopter is made from a 1.5-mm carbon fiber plate cut through computer numerical control. The flapping mechanism is a spatial four-bar mechanism driven by a two-stage reduction gear to realize the reciprocating motion of the wing. The wing membrane is made of polyester fabric. The flight avionics include the main control board, driver board, a Global Positioning System unit, and receiver. The control board is based on an STM32F405RGT6 microcontroller and is connected to a barometer and inertial measurement unit. The driver board is a non-inductive square wave controller based on an STM32F030 microcontroller. All components of the ornithopter are powered by a 300-mAh Li-ion rechargeable battery. Details of the other components are given in Table III. Our robot is similar to its bionic counterpart in terms of wingspan and weight. To eliminate the effect of the tail, the ornithopter has no elevator or rudder, and only has a vertical stabilizer to achieve yaw stability.

TABLE III
COMPONENTS DATA OF THE ORNITHOPTER

Component Name	Weight (g)	Proportion
BLDC motor	9.0	6%
Battery	16.8	11.2%
Gear box	18.5	12.3%
Main Control Board	10.0	6.6%
Driver Board	5.7	3.8%
GPS	6.6	4.3%
Receiver	8.7	5.8%
Compliant Revolute Joint	9.0	6%
Body frame	66	44%
Total	150	100%

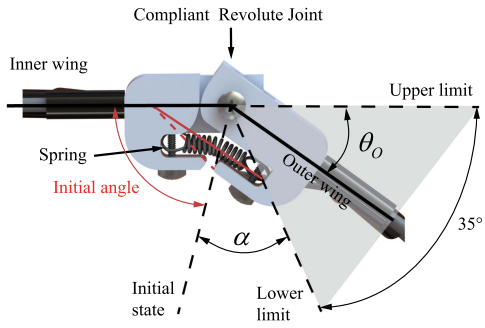

Fig. 4. Schematic diagram of the compliant revolute joint.

C. Compliant Revolute Joint

As shown in Fig. 4, the customized CRJ comprises a carbon-fiber leading edge with a compliant spine. This structure allows asymmetry of the downstroke and upstroke to simulate a revolute joint with a restoring torque on the upstroke. The bending angle is adjusted by the stiffness of the spring. Considering off-the-shelf springs, we chose springs with a length of 10 mm and wire diameters of 0.3, 0.4, and 0.5 mm, with the material being spring steel. The stiffness coefficients are 0.1576, 0.5902 and 1.8145 Nm/rad, labelled $k1$, $k2$ and $k3$, respectively. We introduced a constraint angle α to limit the maximum flapping angle of the outer wing to 35° [19].

III. DYNAMIC MODEL

In this section, we analyze the longitudinal flight dynamics by simplifying the ornithopter model as a mass point model, and we adopt flat plate theory to model the aerodynamics. In addition, the leading edge of the wing is simplified as a double-pendulum with spring system. The models are established to determine the factors of passive wing deformation that affect the maneuverability of an ornithopter.

A. Longitudinal Flight Dynamics

To investigate the effect of the passive morphing of the wings on the pigeon-inspired ornithopter flight, we first develop a dynamic model for the longitudinal flight of the ornithopter. This model is obtained by simplifying the long-term flying function, neglecting the effects of passive deformation of the tail and wing membrane, abstracting the wing as a rigid body, and treating the

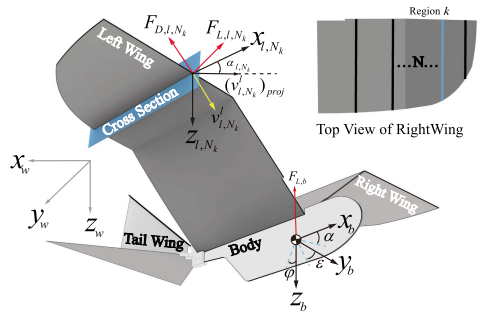

Fig. 5. Dynamic model of the ornithopter in longitudinal flight. Inset: top view division of the right wing.

wing as two rigid plates whose masses are concentrated in the robot body, as shown in Fig. 5.

Following [20], we analyze the longitudinal acceleration of the ornithopter, which can be expressed as the three components $\vec{x}_b$, $\vec{y}_b$, $\vec{z}_b$ of the body:

$$\vec{\alpha}_b = \dot{V}\vec{x}_b + \dot{V}cos\varepsilon\vec{y}_b + \dot{\varphi}V\vec{z}_b, \tag{1}$$

where $\dot{V}$ is the change in the velocity of the ornithopter and $\dot{\varphi}$ is the change in the longitudinal deflection angle. The force $\vec{F}_b$ acting on the ornithopter in the fixed wind frame is expressed as the combined force of the lift of the body $F_{L,b}$, drag of the body $F_{D,b}$, and weight W:

$$\begin{aligned}\vec{F}_b = &[-F_{D,b} - W\sin\alpha]\vec{x}_b + [-F_{L,b}\sin\varepsilon]\vec{y}_b \\ &- [F_{L,b} - W\cos\varphi]\vec{z}_b,\end{aligned} \tag{2}$$

where α is the angle of attack, ε is the lateral deflection angle, and φ is the longitudinal deflection angle. Here, we make the simplification that, in the case of little wind, the longitudinal deflection angle φ is the same as the angle of attack. We combine (1) and (2) to obtain the dynamic model

$$\vec{\alpha}_b = \begin{pmatrix} \dot{V} \\ \dot{V}\cos\varepsilon \\ \dot{\varphi}V \end{pmatrix} = \begin{pmatrix} -\frac{F_{D,b}}{m} - g\sin\alpha \\ \frac{F_{L,b}\sin\varepsilon}{m} \\ \frac{F_{L,b}\cos\varepsilon}{m} - g\sin\alpha \end{pmatrix}. \tag{3}$$

It is therefore seen that the acceleration, used to measure maneuverability, in the $\vec{x}_b$ direction is affected by the drag F_D, whereas that in the $\vec{y}_b$ direction and that in the $\vec{z}_b$ direction are affected by the lift F_L.

B. Aerodynamics

As outlined above, the effect of the lift F_L on the flapping wing in two directions is derived from the dynamic model, and we thus build a more detailed aerodynamic model to investigate which factors affect the lift F_L and drag F_D.We adopt strip theory to divide the left and right wings of the ornithopter into N regions along the span [21], whereas the experiments and calculations in this letter divide the wing area into five strips. It is generally accepted that the center of mass distribution of the ornithopter wing is at the quarter chord and therefore all velocity, acceleration, and force calculations are standardized at the quarter chord. Taking the left wing as an example, the angle of attack is expressed as

$$\alpha_{l,N_k} = \alpha\tan 2\left(v^x_{l,N_k}, v^z_{l,N_k}\right), \tag{4}$$

where α_{l,N_k} is the angle of attack in the divided region k of N on the left wing, v^x_{l,N_k} is the velocity in the divided region k of the left-wing velocity v^l_{l,N_k} in the x direction along the vertical component of the wing, and v^z_{l,N_k} is the velocity component in that direction. The derivation is the same for the right wing. The lift and drag of the left wing are expressed as

$$\begin{aligned} F_{L,l,N_k} &= \frac{1}{2}C_L\rho A_{l,N_k}\left\|\left(v^l_{l,N_k}\right)_{proj}\right\|^2 \\ F_{D,l,N_k} &= \frac{1}{2}C_D\rho A_{l,N_k}\left\|\left(v^l_{l,N_k}\right)_{proj}\right\|^2, \end{aligned} \tag{5}$$

where C_L and C_D are the lift and drag coefficients respectively, ρ is the air density, and $(v^l_{l,N_k})_{proj}$ is the velocity projected of the section in divided region k. A_{l,N_k} is the effective area in divided region k of N on the left wing:

$$A_{l,N_k} = \frac{(L_C)_{proj}(L_S)_{proj}}{N}, \tag{6}$$

where $(L_C)_{proj}$ and $(L_S)_{proj}$ are the length of the wing chord and the length of the wingspan projected in the horizontal direction respectively. There are two factors affecting the lift and drag, namely the angle of attack and effective wing area.

C. Double Pendulum with Spring System

The projected lengths of the wing chord $(L_C)_{proj}$ and wingspan $(L_S)_{proj}$ are directly affected by the flapping angle. The muscles of the forearm play an important role in pigeon flapping flight, producing a combined movement of the shoulder, elbow, and wrist that changes the wing shape for different flight conditions. In terms of the anatomy of a pigeon, the patagium longus and extensor carpi muscles are attached to the first digit and carpometacarpus and function to flex the elbow. In contraction during flapping, the patagium longus and extensor carpi muscles stretch the first digit and carpometacarpus, thus moving the wrist as shown in Fig. 6. In addition, the pressure differential between the upper and lower surfaces of the wing affects the wing shape [22], [23], [24]. This asymmetry effectively prevents lift canceling, allowing the pigeon to fly well.

The above mechanism inspires us to simplify the design of the muscle stretch by inserting a CRJ at the leading edge of the wing. The inner wing section has fixed restraints and is attached to the link lever at the wing root on one side and to the CRJ on the other, whereas the outer wing section has only one attachment to the CRJ. As a result, the leading edge of the wing bending during the upstroke and straightens during the downstroke just like for a pigeon. Pigeons change their wing shape by varying the stretch of their muscles, and we thus use three springs with different stiffness to mimic the changes under different flight conditions.

The elasticity coefficient of the CRJ C_T is thus expressed as

$$C_T = \frac{\mathrm{d}F_T}{\mathrm{d}\phi}, \tag{7}$$

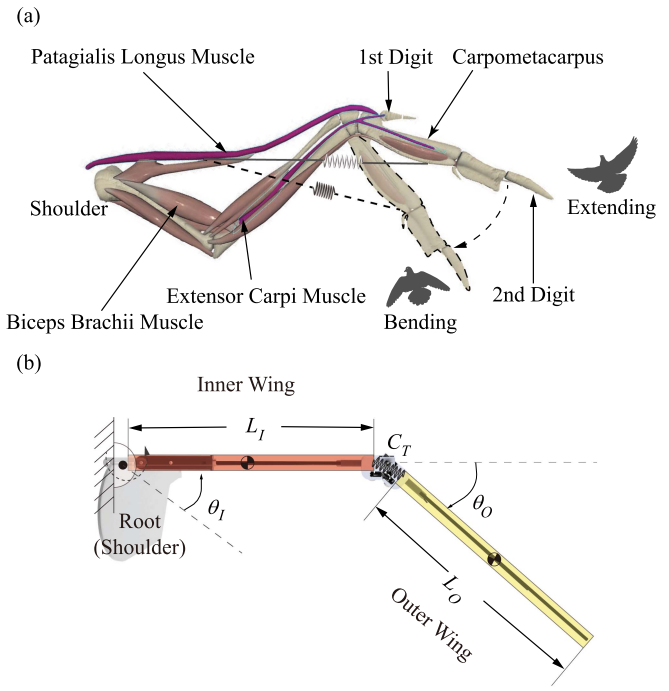

Fig. 6. Model of the leading edge of the wing system: (a) muscle and skeletal illustration of the pigeon forearm while bending; (b) system of a double pendulum connected by a spring.

where F_T is the tension force acting on the spring and ϕ is the angle of deformation of the spring after receiving the tension force. Here, we use three springs with different stiffness, individually tested and applied to the CRJ. The Lagrange method $L = T - V$ is used to solve the double-pendulum model of the leading edge of the wing, and we therefore obtain the relationship between C_T and θ_O for the angle between the rigid rod of the outer wing and the horizontal direction:

$$\ddot{\theta}_O = \frac{J_3\left(\ddot{\theta}_I \cos\theta_O - \dot{\theta}_I\dot{\theta}_O\right)}{J_2} + \frac{\mu_2 \cos(\theta_O - \theta_I)}{J_2} - \frac{C_T(\theta_O - \theta_I)}{J_2} - \ddot{\theta}_I, \tag{8}$$

where θ_I is the swing angle of the inner wing, and $J_3 = \frac{1}{2}m_3 L_I L_O$, $J_2 = \frac{1}{3}m_3 L_O^2$, $\mu_2 = \frac{1}{2}m_3 g L_O$. All the equations are derived by simplifying the Lagrange equation. The lengths of the inner wing rod and outer wing rod, L_I and L_O, are measured directly, whereas θ_I and θ_O are calculated in post-processing with motion capture software. We thus conclude that the spring stiffness directly affects the angle of passive bending and thus the effective wing area.

The longitudinal dynamic model shows that the lift, which determines maneuverability, is mainly determined by the angle of attack and effective wing area. On the basis of the discussion in Section IV-B, we determine which of the two factors is dominant.

IV. Experimental Validation

Using the equations from the previous section, this section presents the effect of the spring-assisted bending wing on flight kinematics, lift/thrust, and power consumption. In addition, in further exploring the compliant hinge properties, the double-pendulum model with a spring is used to establish the quantitative relationship between the spring stiffness and passive bending angle.

A. Experimental Setup

An Opti-Track motion capture system with eight cameras was used to record the flapping kinematics and passive bending angle of the robot's wings. We divided each wing into four equal parts of 7.5 cm and then fitted 37 reflective markers on the leading edge, trailing edge, and quarter chord along the wing section. We recorded the thrust force and lift using an analogue six-axis force/torque sensor (M4312 G). This sensor has a resolution of 0.01 N. In addition, an 8.4 V DC power supply (eTM-305P) was used to drive a brushless motor (GR1404) through an electronic speed controller. A digital multimeter (DMM7510, KEITHLEY) simultaneously measured the drive current for calculations of power consumption. During the experiments, we ran the motion capture system, the load cell sensor and the DMM were sampled at a rate of 200 Hz, and the data were smoothed using a moving average filter and fourth-order Butterworth filter. The RC receiver received the signal from the remote control and controlled the electronic speed controller to generate four flapping frequencies between 3 and 6 Hz [25], which were suitable for free flight. Data were collected for at least 5 s when the flapping frequency was stable. In total, 16,000 frames of data were obtained for three sets of deformable wings and one set of rigid wings.

B. Wing Kinematics

In this letter, the stroke plane is defined as the path of the wing tip from the lateral view of the ornithopter, and the stroke angle θ is that between the inclination of the leading-edge spar and a horizontal reference. The spanwise twist angle β_i ($i = 1,..,4$) is defined as the difference in the angle of incidence between a spanwise location and a 20% sspanwise location, whereas the angle of incidence (sometimes referred to as the geometric angle of attack) is defined as the angle between a chord line and the stroke plane. The angle of attack (AoA) α_i ($i = 1,..,4$) is defined as that between a chord line and the relative wind speed vector of a wing section, and the wind velocity vector is obtained from the second-order central difference of the quarter chord in the last and next time steps. In general, we use the above four metrics to measure the effects of different spring coefficients on the flapping wing kinematics (Fig. 7).

Considering the effect of frequency on the flapping-wing kinematics, Fig. 7(a) shows that the stroke angle of the rigid wing decreases by 6° as the flapping frequency increases. However, the stroke angle of the spring-assisted flexible wing is almost constant at the designed 96°, being largely independent of the wingbeat frequency. As observed, the stroke angles of the flexible wing labelled $k2$ changes less with the flapping frequency, and the spring-assisted flexible wing thus effectively maintains the stroke angle. In Fig. 7(b), the twist angle of both the rigid and flexible wings increases with increasing flapping frequency

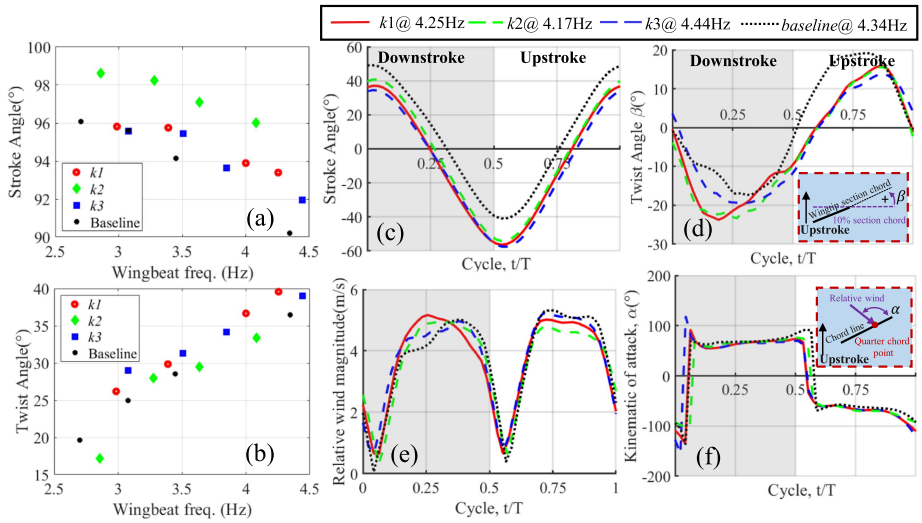

Fig. 7. Effect of the spring stiffness coefficient on the frequency-dependent flapping wing kinematics: (a) frequency-dependent amplitude of the stroke angle; (b) frequency-dependent amplitude of the wing twist angle; (c)-(f) transient kinetic variables of the wing tip.

owing to the increasing inertial and aerodynamic loads. The lift angle and twist angle increase proportionally with the flapping frequency.

Next, the effect of the spring stiffness on the flapping kinematics is investigated for similar frequency. The measured baseline is a rigid wing with the same mass as the compliant-joint flexible wing. Fig. 7(d) to (f) shows that the wing kinematics do not change greatly with the inclusion of the CRJ, except that the amplitude of the upstroke and downstroke decreases by 20°, owing to the limit of the CRJ. Furthermore, the twist angle of the flexible wing remains the same as that of the rigid wing, with the difference being that the twist angle of the flexible wing increases by 5° during the downstroke and decreases by 5° during the upstroke. Interestingly, Fig. 7(f) shows that the angles of attack of the rigid and flexible wings are the same, the amplitudes of the upstroke and downstroke remain at 100°, and the spring stiffness has little effect on the angle of attack.

C. Lift/Thrust Generation and Power Consumption

Fig. 8(a) shows the frequency dependence of the mean thrust, indicating the effect of inertial forces. As the flapping frequency increases, the thrust increases for all four sets of wings, and the spring stiffness has less effect on the thrust. As described earlier, owing to the constant twist angle, the average thrust of a flexible wing is approximately the same as that of a rigid wing. For example, at a flapping frequency of approximately 4.1 Hz, the three sets of flexible wings produce almost the same mean thrust; i.e., 40.1547 g, 45.1203 g, and 35.6265 g. Meanwhile, the mean thrust of the rigid wing is 27.6756 g (Fig. 8(d)).

The effect of the spring stiffness on the frequency-dependent lift is more obvious. Fig. 8(b) shows that, unlike a flexible wing, the average lift of the rigid wing increases slowly as the flapping frequency increases. As an example, at a flapping frequency of 4.4 Hz, the average lift generated by the four wing types is 255.3568 g for the rigid wings and 229.918, 271.7765 and

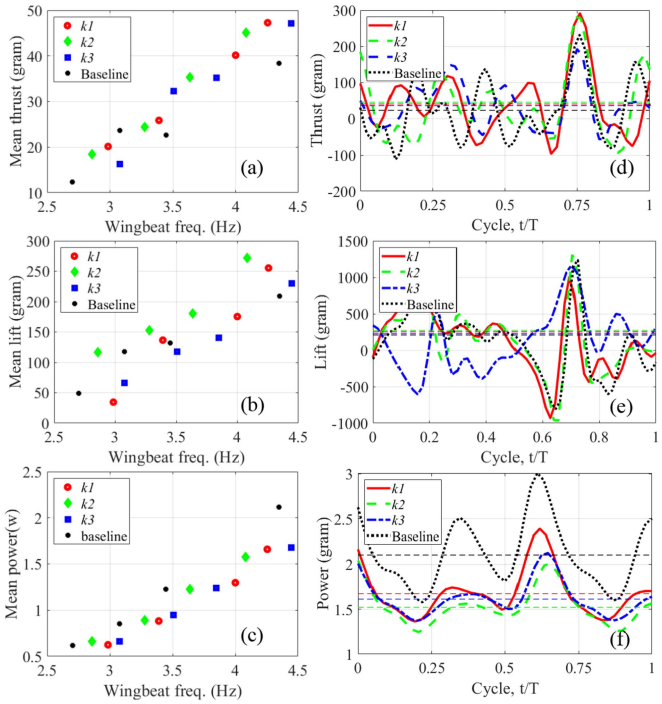

Fig. 8. Effects of compliant joint on lift/thrust generation and power consumption: (a)-(c) frequency dependence of mean lift/thrust and power consumption; (c)-(d) transient of lift/thrust and power consumption.

208.8018 g for the flexible wings. This means that at a similar flapping frequency, the deformable wing labelled $k2$ has 22.3% more lift than the rigid wing. The mean lift of the flexible wing labelled $k2$ is 1.8 times the take-off weight (150 g). This is due to the passive bending angle, which is covered in detail in the next part.

The power consumption gradually increases with the flapping frequency. As expected, more power is required to drive the rigid wings. However, the stiffness of the springs has little effect on

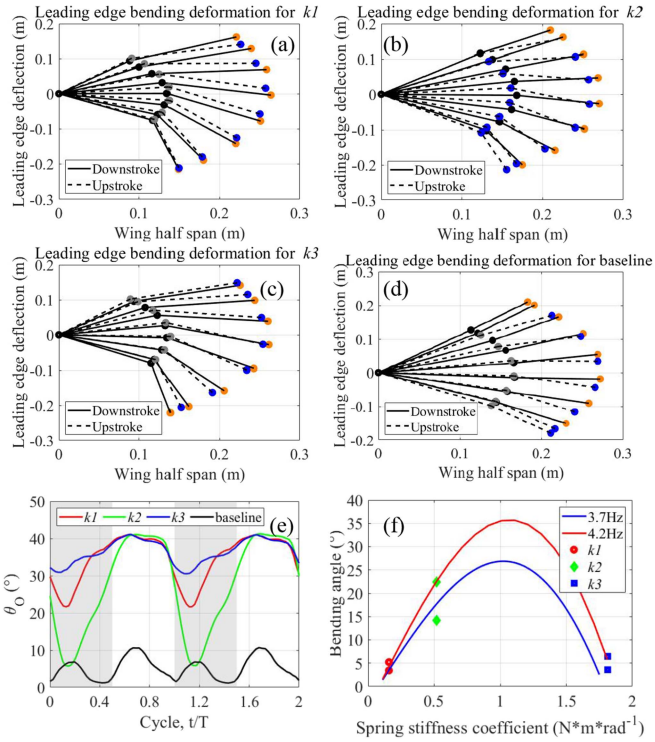

Fig. 9. Effect of the spring stiffness coefficient on the bending angle: (a)-(d) passive bending deflection of the leading-edge spar; (e) schematic of the bending angle; and (f) effect of the spring stiffness coefficient on the bending angle.

the power consumption. Fig. 8(c) shows that wings equipped with the three springs of different stiffness have almost the same energy consumption at similar flapping frequencies. This is because the compliant joint converts inertial energy into spring potential energy and releases it at the right time, effectively reducing energy consumption. Fig. 8(e) and (f) show the transients in lift production and power dissipation when the flapping frequency is approximately 4.4 Hz. The rigid wing produces average lift of 208.8 g and consumes 2.1 W of electrical power. At the same flapping frequency, the flexible wing labelled $k2$ produces 271.77 g of lift and consumes only 1.52 W of electrical power. This is an energy saving of 38.2%.

Compared with SmartBird [14], which uses 18 W of electrical power to generate 3 N of lift through the active bending of wings, our robot has a lower power-to-take-off weight ratio (0.010 vs. 0.038) and a higher lift-to-take-off weight ratio (1.81 vs. 0.625). This means that in addition to saving energy, our proposed solution generates more lift without introducing additional actuators. These improvements were made possible by fabricating the prototype using biological data and modeling muscle through the spring stiffness.

D. CRJ Properties

Fig. 9(e) shows that an appropriate setting of stiffness effectively increases the bending angle and thus the lift. As an example, when the flapping frequency is 4.2 Hz, the bending angle of the flexible wing labelled $k2$ is 35°, which reduces the length of wingspan by 18.1%, whereas the bending angles

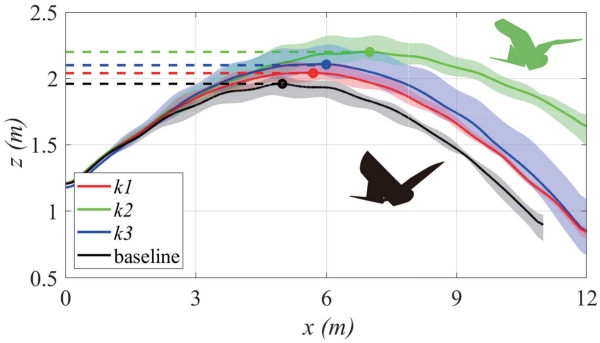

Fig. 10. Free flight trajectory of the ornithopter. The plots show the mean value and variance for three sets of flight.

of the other two sets of flexible wing with different stiffness coefficients (labelled $k1$ and $k3$) are 18° and 10°, respectively. As the initial bending angle is zero, the bending angle of the rigid wing fluctuates around 0° by approximately 8°. To further obtain the quantitative relationship between the stiffness coefficient and bending angle, we use the stroke angle of the inner wing at 4.2 Hz as the input to (8) to obtain the optimal stiffness coefficient of 1.11 Nm/rad. Of course, this stiffness is frequency dependent. When the flapping frequency is reduced to 3.7 Hz, the optimal stiffness coefficient becomes 1.02 Nm/rad.

As described in Section III-B, there are two factors that affect wing lift, namely the angle of attack and effective wing area. In (5), the lift and drag coefficients, C_L and C_D, are functions of only the angle of attack, and the kinematic analysis of Section IV-B shows that the angle of attack is not affected by the CRJ in the bending of the wings. Therefore, the main way to increase the mean lift of passively bending wings is to reduce the effective area on the upstroke. This conclusion is verified by the asymmetric leading-edge spar in the upstroke and downstroke in Fig. 9(a)–(d).

E. Free Fight Test

We performed a free flight test in the same environment used to collect the experimental pigeon flight data and thus evaluate the function of the passive bending wing. The ornithopter was fitted with a reflective marker 5 cm above the shoulder. In this test, the robot with rigid wings or one of three sets of passive bending wings was launched by a catapult-assisted launch platform at approximately 4 m/s. During the flight, the throttle was set to produce a flapping frequency of roughly 5 Hz. The throttle was reduced when the flight reached a stable altitude to protect the prototype.

Fig. 10 shows that, compared with the ornithopter with rigid wings (1.96 m), the ornithopter with passive bending wings had higher stable climb heights (2.04, 2.2, and 2.104 m). This means that reducing the upstroke drag increases the mean lift and ultimately achieves the purpose of increasing flight acceleration. The experiment illustrated the effective use of passive bending wings for flight maneuverability.

Specifically, as shown in the multimedia material, an asymmetry in length between the left and right wings, combined

with a small spring stiffness error, generated a rolling moment in flight [13]. We will further consider more technical specifications to quantitative assess our robot, such as stability and agility, etc. Moreover, we will also analyze the effect of wind disturbance and battery size on flight performance.

V. Conclusion

This study investigated the effect of passive wing bending on the lift of an ornithopter. Leveraging simplified longitudinal flight dynamics equations and flat plate theory and using a double-pendulum model with a spring, we studied the dynamics of an ornithopter with flexible wings. Our results show that the lift was determined by the angle of attack and the effective wing area, and the stiffness coefficient of the CRJ determined the bending angle and ultimately the effective wing area.

A prototype of the ornithopter was designed using biological data. Results of the wing kinematics, lift/thrust generation, power consumption, and CRJ properties show that the flexible wing effectively maintains the wing kinematics. In addition, the effective wing area during the upstroke can be reduced to increase the mean lift, assuming that the angle of attack remains unchanged. In flight experiments, an ornithopter with flexible wings had a higher stable climb height, demonstrating an improvement in maneuverability.

Acknowledgment

The experimental protocol was discussed and agreed in advance with the Ethical Committee of Institute of Zoology, Chinese Academy of Sciences.

References

[1] J. A. Cheney et al., "Raptor wing morphing with flight speed," *J. Roy. Soc. Interface*, vol. 18, no. 180, 2021, Art. no. 20210349.

[2] I. G. Ros, P. S. Bhagavatula, H.-T. Lin, and A. A. Biewener, "Rules to fly by: Pigeons navigating horizontal obstacles limit steering by selecting gaps most aligned to their flight direction," *Interface Focus*, vol. 7, no. 1, 2017, Art. no. 20160093.

[3] V. Baliga, I. Szabo, and D. Altshuler, "Range of motion in the avian wing is strongly associated with flight behavior and body mass," *Sci. Adv.*, vol. 5, no. 10, 2019, Art. no. eaaw6670.

[4] A. K. Stowers, L. Y. Matloff, and D. Lentink, "How pigeons couple three-dimensional elbow and wrist motion to morph their wings," *J. Roy. Soc. Interface*, vol. 14, no. 133, 2017, Art. no. 20170224.

[5] D. Lentink et al., "How swifts control their glide performance with morphing wings," *Nature*, vol. 446, no. 7139, pp. 1082–1085, 2007.

[6] Z. Hasnain, J. E. Hubbard Jr, J. Calogero, M. I. Frecker, and A. A. Wissa, "Understanding the relationship between pitch agility and propulsive aerodynamic forces in bio-inspired flapping wing vehicles," in *Proc. Smart Mater., Adaptive Struct. Intell. Syst.*, 2015, Art. no. V002T06A001.

[7] U. M. Norberg, "Evolution of vertebrate flight: An aerodynamic model for the transition from gliding to active flight," *Amer. Naturalist*, vol. 126, no. 3, pp. 303–327, 1985.

[8] C. Harvey, V. Baliga, P. Lavoie, and D. Altshuler, "Wing morphing allows gulls to modulate static pitch stability during gliding," *J. Roy. Soc. Interface*, vol. 16, no. 150, 2019, Art. no. 20180641.

[9] D. R. Warrick, M. Bundle, and K. Dial, "Bird maneuvering flight: Blurred bodies, clear heads," *Integrative Comp. Biol.*, vol. 42, no. 1, pp. 141–148, 2002.

[10] C. Harvey, L. L. Gamble, C. R. Bolander, D. F. Hunsaker, J. J. Joo, and D. J. Inman, "A review of avian-inspired morphing for UAV flight control," *Prog. Aerosp. Sci.*, vol. 132, 2022, Art. no. 100825.

[11] D. Warrick and K. P. Dial, "Kinematic, aerodynamic and anatomical mechanisms in the slow, maneuvering flight of pigeons," *J. Exp. Biol.*, vol. 201, no. 5, pp. 655–672, 1998.

[12] H. Tanaka, T. Nakata, and T. Yamasaki, "Biomimetic soft wings for soft robot science," *J. Robot. Mechatron.*, vol. 34, no. 2, pp. 223–226, 2022.

[13] D. Billingsley, G. Slipher, J. Grauer, and J. Hubbard, "Testing of a passively morphing ornithopter wing," in *Proc. AIAA Infotech, Aerosp. Conf. AIAA Unmanned. Unlimited Conf.*, 2009, Art. no. 1828.

[14] W. Send, M. Fischer, K. Jebens, R. Mugrauer, A. Nagarathinam, and F. Scharstein, "Artificial hinged-wing bird with active torsion and partially linear kinematics," in *Proc. 28th Congr. Int. Council Aeronautical Sci.*, 2012, pp. 10–20.

[15] Y. Tummala, A. Wissa, M. Frecker, and J. E. Hubbard, "Design and optimization of a contact-aided compliant mechanism for passive bending," *J. Mechanisms Robot.*, vol. 6, no. 3, 2014, Art. no. 031013.

[16] C. Ruiz, J. Á. Acosta, and A. Ollero, "Optimal elastic wing for flapping-wing robots through passive morphing," *IEEE Robot. Automat. Lett.*, vol. 8, no. 2, pp. 608–615, Feb. 2023.

[17] E. Ajanic, A. Paolini, C. Coster, D. Floreano, and C. Johansson, "Robotic avian wing explains aerodynamic advantages of wing folding and stroke tilting in flapping flight," *Adv. Intell. Syst.*, vol. 5, no. 2, 2022, Art. no. 2200148.

[18] J. P. Calogero, M. I. Frecker, Z. Hasnain, and J. E. Hubbard Jr, "Dual optimization of contact-aided compliant mechanisms for passive dynamic shape change," *AIAA J.*, vol. 56, no. 9, pp. 3745–3756, 2018.

[19] X. Fan, K. Breuer, and H. Vejdani, "Wing fold and twist greatly improves flight efficiency for bat-scale flapping wing robots," in *Proc. IEEE/RSJ Int. Conf. Intell. Robots Syst.*, 2021, pp. 7391–7397.

[20] E. Ajanic, M. Feroskhan, S. Mintchev, F. Noca, and D. Floreano, "Bioinspired wing and tail morphing extends drone flight capabilities," *Sci. Robot.*, vol. 5, no. 47, 2020, Art. no. eabc2897.

[21] A. Ramezani, S.-J. Chung, and S. Hutchinson, "A biomimetic robotic platform to study flight specializations of bats," *Sci. Robot.*, vol. 2, no. 3, 2017, Art. no. eaal2505.

[22] K. M. Kage, "A portrayal of biomechanics in avian flight," M.S. thesis, College Health Sci. Technol., Rochester Inst. Technol., Rochester, NY, USA, 2014.

[23] R. J. Vazquez, "Functional anatomy of the pigeon hand (*columba livia*): A muscle stimulation study," *J. Morphol.*, vol. 226, no. 1, pp. 33–45, 1995.

[24] A. M. B. Robertson and A. A. Biewener, "Muscle function during takeoff and landing flight in the pigeon (*columba livia*)," *J. Exp. Biol.*, vol. 215, no. 23, pp. 4104–4114, 2012.

[25] P. Nian, B. Song, J. Xuan, W. Zhou, and D. Xue, "Study on flexible flapping wings with three dimensional asymmetric passive deformation in a flapping cycle," *Aerosp. Sci. Technol.*, vol. 104, 2020, Art. no. 105944.